



An assessment of the impact of surface currents on wave modeling in the Southern Ocean

Henrique Rapizo^{1,2} · Tom H. Durrant² · Alexander V. Babanin¹

Received: 24 July 2017 / Accepted: 16 May 2018 / Published online: 26 May 2018
© Springer-Verlag GmbH Germany, part of Springer Nature 2018

Abstract

This paper presents an assessment of the impact of the ocean circulation on modeled wave fields in the Southern Ocean, where a systematic positive bias of the modeled wave height against altimetry data has been reported. The inclusion of ocean currents in the wave model considerably reduces the positive bias of the simulated wave height for high southern latitudes. The decrease of wave energy in the presence of currents is almost exclusively related to the reduction of the relative wind, caused by an overall co-flowing current field associated with the Antarctic Circumpolar Current. Improvements of the model results are also found for the peak period and the mean period against a long-term moored buoy. At the mooring location, the effect of currents is greater for larger and longer waves, suggesting remotely generated swells are more influenced by the currents than local waves. However, an additional qualitative analysis using high-resolution currents in a finer grid nested to the global coarser grid shows that typical resolution of global hydrodynamic reanalysis is not sufficient to resolve mesoscale eddies, and as a consequence, the simulation of mesoscale wave patterns can be compromised. The results are also discussed in terms of the accuracy of forcing fields.

Keywords Wind-generated waves · Deep water wave modeling · Wave–current interactions · Relative wind

1 Introduction

Current-induced effects on waves have been extensively investigated in coastal regions, where currents are usually strong and highly variable in space and time. In tide-dominated environments, for example, it has been shown that currents can modulate significantly the main wave parameters at the tide frequency (e.g., Tolman 1990). However, in large ocean basins, the degree to which currents modify the wave field requires further investigation, theoretical approaches prevail, and observations of the effects of currents on the wave field are scarce. The spatio-temporal variability of currents in relation to typical wave scales is larger in deep water compared to that in coastal environments. Nevertheless, previous works suggest that mesoscale currents can have

a large effect on the waves due to refraction (e.g., White and Fornberg 1998; Ardhuin et al. 2017). Furthermore, the moving water surface affects the relative wind speed (Hersbach and Bidlot 2008), which can reduce or increase the momentum flux from wind to waves in conditions of following or opposing currents, respectively.

The effects of currents on deep water waves can be broadly separated into two categories: generation and propagation. There is a lack of studies on how a moving medium modifies the process of wave generation. A notable exception of observations with wave growth in regions with strong currents is the work of Haus (2007), where results indicate that the relative or “effective” wind speed and a shift of the wind stress away from the mean wind direction can modify wave growth conditions. The modulation of wind stress was inferred by Drennan and Shay (2006) as being caused by the direction shift of the short wave components that support most of the stress. Based on the geometrical optics approximation, Kenyon (1971) concluded that the effects of refraction and related processes can be significant over mesoscale circulation features. Kudryavtsev et al. (1995) provided direct observations of refraction-induced effects on the wave field in the Gulf Stream frontal zone.

Responsible Editor: Sandro Carniel

✉ Henrique Rapizo
h.rapizo@metocean.co.nz

¹ Department of Infrastructure Engineering, University of Melbourne, Victoria, Australia

² MetOcean Solutions, Raglan, New Zealand

Numerical modeling provides a valuable tool for investigating and understanding the interaction of waves with surface currents. In the nearshore, due to the higher complexity of this interaction, the two-way coupling of hydrodynamic and wave models has been shown to bring improvements in the simulation of wave conditions (e.g., Benetazzo et al. 2013; Bolaños et al. 2014). However, the impact of currents on the large-scale wave field has received relatively little attention.

The development of spectral wave models has led to highly accurate simulations of integrated wave parameters. Validation and calibration of model results on global scales using satellite altimeter data have contributed to significant improvements to model source terms (e.g., Ardhuin et al. 2010; Zieger et al. 2015). With the exception of peak period and direction, the simulation of spectrally integrated parameters generally agrees well with available measurements (e.g., Stopa et al. 2016). However, there are regions where the model still produces persistent biases in significant wave height H_s and mean wave period, notably in the Southern Ocean (e.g., Rapizo et al. 2015).

A number of authors have reported the presence of a positive bias in modeled H_s in the Southern Ocean (SO) against altimeter data (e.g., Ardhuin et al. 2015; Zieger et al. 2010; Durrant et al. 2013) using the WAVEWATCH III model (WW3 Tolman 1991). Recently, Rapizo et al. (2015) showed that a similar result is found for a long-term moored buoy, with considerable biases also for the peak period T_p and the mean period T_{m01} . The purpose of this study is to investigate the current-induced effects on waves in the SO and the relative impact they have on the biases of main wave parameters.

The SO has an important contribution to the global wave climate (Alves 2006). The absence of land barriers and constant strong winds make the SO one of the main sources of high-energy and long-period swells to all other major oceans. At the high southern latitudes, the Antarctic Circumpolar Current (ACC) runs with the predominant westerly winds and, consequently, with the resultant mean wave direction. This represents an interesting opportunity to investigate and understand how the consistent eastward mean flow impacts the wave generation and propagation over this vast oceanic area.

The paper is laid out as follows: Section 2 briefly reviews the approach used in spectral wave models to account for current-induced effects, the methods employed are described in Section 3 including wave and hydrodynamic models and the data set used, and results of the SO modeling are presented in Section 4. In Section 4.3, the potential impact of currents on wave refraction is investigated. The possible influence of a mesoscale eddy on the wave field around the SOFS is analyzed in terms of convergence/divergence of the wave energy, which aims to

give a qualitative sense of the intensity of wave refraction on mesoscale hydrodynamic features. The accuracy of forcing fields of wind and current is discussed in Section 5. Lastly, concluding remarks are given in Section 6.

2 Effects of currents in spectral wave models

Third-generation spectral wave models operate on some form of the radiative transfer equation (RTE) or conservation of wave action. The wave action spectral density $N = E/\sigma$, where E is the spectral energy density and σ is the wave radian frequency, will vary in space \mathbf{x} , time t , and wavenumber and wave direction spaces, i.e., $N(\mathbf{x}, t; k, \theta)$, according to (e.g., Tolman 1991)

$$\frac{\partial N}{\partial t} + \nabla_{\mathbf{x}} \cdot [(\mathbf{U} + \mathbf{c}_g)N] - \frac{\partial}{\partial k} \left(\mathbf{k} \cdot \frac{\partial \mathbf{U}}{\partial s} N \right) + \frac{\partial}{\partial \theta} \left(\frac{1}{k} \mathbf{k} \cdot \frac{\partial \mathbf{U}}{\partial m} N \right) = \frac{S_{tot}}{\sigma}, \quad (1)$$

where \mathbf{c}_g is the wave group velocity in a frame of reference moving with the current $\mathbf{U}(\mathbf{x}, t)$, s and m are coordinates parallel and orthogonal to the \mathbf{k} -vector, and S_{tot} comprises non-conservative processes and wave-wave nonlinear interactions. Since our interest is in deep water large scale modeling, depth-induced effects were disregarded in Eq. 1. The left-hand side of Eq. 1 describes the wave kinematics and dynamics. It is assumed that the current field varies slowly in space and time with respect to wavelength and wave period, respectively, which is a reasonable approximation in most situations where the hydrodynamics are controlled by tides or geostrophic balance (Peregrine 1976). The right-hand side of Eq. 1 represents the positive and negative source of energy as well as its distribution in spectral space. The wave action is a property that, unlike wave energy E , is conserved along a wave packet path (Bretherton and Garret 1969), which makes it more suitable for spectral wave modeling.

The kinematic equations are modified when applying the frequency Doppler shift, i.e., $\sigma = \omega - \mathbf{k} \cdot \mathbf{U}$, where ω is the absolute frequency or the frequency in a frame of reference moving with the Earth. The total velocity at which the wave action is advected in space becomes directly proportional to the currents, i.e. $\mathbf{U} + \mathbf{c}_g$. The wavenumber changes as a function of current spatial gradients in the wavenumber direction $\partial \mathbf{U} / \partial s$ and, as a consequence, waves are refracted by transverse current gradients $\partial \mathbf{U} / \partial m$. In known current fields and in conditions where the wave linear dispersion applies, the wave kinematics are well simulated by the action balance equation (e.g., Chawla and Kirby 2002). However, the model accuracy is compromised in opposing currents and near blocking regions

(Van der Westhuysen 2012; Ardhuin et al. 2012; Rapizo et al. 2017) where nonlinearities play an important role in the wave-current interactions (e.g., Chawla and Kirby 2002; Babanin et al. 2011).

A consequence of the conservation of wave action $E/\sigma(k)$ is that if waves propagate over collinear currents with negative (positive) shear in the along wave direction, they will experience increase (decrease) in wavenumber and, consequently, in wave energy. Additionally, refraction-induced convergence and divergence of wave energy have been shown to be important factors in modulating the spatial distribution of wave height on the mesoscale (Ardhuin et al. 2017). One of the most evident examples of wave refraction is wave trains propagating over mesoscale ocean eddies. Due to the inverted horizontal current shear, one side of the eddy diverges the incoming wave rays, whereas the other side converges the rays (e.g., Mathiesen 1987). Rapizo et al. (2014) showed numerically that eddy scales as observed from global reanalysis can potentially create this effect on Southern Ocean swells.

The forcing terms S on the right-hand side of Eq. 1 has been historically subgrouped by the energy input from the wind S_{in} , dissipation (wave breaking, bottom friction, and others) S_{ds} , and nonlinear wave–wave interactions S_{nl} . The last two terms remove and redistribute energy in the spectral space, respectively. Although the development of wave models has been primarily performed by improving the parameterization of these processes, surprisingly, currents are considered only in the S_{in} term. Nonlinear interactions and dissipation by breaking do not directly take into account the mean water flow. Nonlinear interactions and the development of a spectral tail, for example, can be perturbed if the current field is highly variable (Waseda et al. 2015; Rapizo et al. 2016). By entering opposing currents, wave breaking probability increases as a consequence of wave steepening (Chawla and Kirby 2002). In such conditions, spectral wave models fail in representing the dissipation rate, which leads to the overestimation of wave energy (Ardhuin et al. 2012; Rapizo et al. 2017; Ris and Holthuijsen 1996; Van der Westhuysen 2012). More observations and modeling tests under such conditions are needed in order to improve parameterizations by including current effects.

The wind input function accounts for the mean current through a somewhat simplified vector balance between the local wind and current, which can be expressed as

$$\mathbf{u}_e(z) = \mathbf{u}(z) - a\mathbf{U}, \quad (2)$$

where $\mathbf{u}(z)$ is the wind vector at a certain level z (as measured by an anemometer, for example), \mathbf{U} is the ocean surface current vector and $\mathbf{u}_e(z)$ is the resultant effective wind vector. The largest effect of currents is found for $a = 1$. This is a simplistic approach, as pointed out by Hersbach and Bidlot (2008), since the currents would act on

the wind stress and consequently influence the atmospheric boundary layer and the whole wind profile. However, a proper account of this effect would require a fully coupled wave–hydrodynamic–atmospheric model.

The wind input term in spectral wave models operates traditionally on the friction velocity u_* , which is parameterized in terms of the wind speed at 10-m height (U_{10}) by considering that the wind profile is logarithmic. Different terms have been proposed to represent the energy input from the wind, which commonly use the factor $u_*/c_p \cos \phi$ (e.g., Komen et al. 1984), where c_p is the wave phase velocity and ϕ is the angle between wind and wavenumber vectors. A wind blowing over a surface in motion will produce a different stress on the water surface. If winds and currents are running in the same direction, the momentum flux to the waves is reduced and the resultant waves are smaller. On the other hand, if waves and currents oppose each other, the wind stress increases and so does the momentum flux from wind to waves.

Therefore, spectral wave models include current-induced effects in a rather simplistic fashion. The implications on the terms of the left hand side of Eq. 1 are all derived from the modified Doppler-shifted frequency. Among the source terms, the effects caused by the presence of currents are included in the wind input term only. The results of the simulations presented in Section 4 will be interpreted and discussed based on the theory given in this section and accounted for in the wave model.

3 Methods

All numerical simulations were performed using the WW3 model version 4.18. This model has been extensively used for global and regional scale hindcasting (e.g., Chawla et al. 2012; Raschle and Ardhuin 2013; Durrant et al. 2014) and is the most widely used operational forecast model for offshore conditions. Although the simulations were performed for the whole globe, our main interest is in the results for the Southern Ocean (SO). The impact of currents on the typical positive bias in H_s will be extensively discussed throughout the paper. It should be noted that this study does not aim to perform a statistical climate analysis. Our goal is to investigate the impact of currents on waves with the focus on the main physical factors responsible for the observed changes and the relevance of using the currently available hydrodynamic reanalysis to wave hindcasts.

The chosen time frame of the analysis is 13 months, from 01-Dec-2011 to 31-Dec-2012. This period includes the second deployment of the Southern Ocean Flux Station (Schulz et al. 2012), which consists of a moored buoy in high southern latitudes (see Section 3.2 for details)

and that will be used in this work. Additionally, satellite altimetry data are used to validate the numerical results. The time frame considered includes various available satellite sources. Satellite data have the advantage of providing spatial fields of wave height over large ocean areas. By using the information obtained from the floating mooring, we can also analyze the response of other wave parameters such as wave period and direction to the inclusion of currents.

The relevance of currents to wave modeling is investigated by validating the performance of the global model in the presence and absence of ocean currents with emphasis on the SO results. In order to separate the effects of currents on wave generation and propagation, the simulations in the presence of currents were performed with two different configurations: with the relative wind effect activated (RWND ON hereafter) and deactivated (RWND OFF) (see Eq. 2). By not considering the vector balance between winds and currents, the momentum flux is unaltered and so is the wind input source. In this case, propagation-related effects represented by a modified group velocity, wavenumber, and refraction are the factors responsible for affecting the wave field. These effects are related, for instance, to changes in wave energy due to straining/stretching of wavelength or refraction-induced focusing/defocusing (see Section 2). An additional simulation is run with high-resolution currents ($1/12^\circ$) interpolated on a finer grid (0.1°). This grid is nested to the global coarse grid and is delimited by the coordinates $135\text{--}145^\circ$ E and $52\text{--}45^\circ$ S. This last simulation is not validated, but instead it aims to qualitatively investigate and provide a discussion on the effects of the current grid resolution on wave refraction. Therefore, a total of four simulations are performed: in the absence of currents, in the presence of currents with RWND activated, in the presence of currents with RWND deactivated, and a last simulation with high-resolution computational grid and current fields nested to the coarser global grid.

For the spatial validation and quantitative assessment of the H_s differences between simulations with and without currents in the Southern Ocean, the statistical analysis is performed within the latitude limits of 30° S– 60° S (Fig. 1). Therefore, although the simulation is performed

using global forcing grids, the analysis of results is focused on the Southern Ocean, which is subdivided into three sectors following the major global oceans (Fig. 1). The statistical variables used to quantify the differences between observed (O) and modeled (M) values are defined as follows: absolute bias $\frac{1}{N} \sum (O - M)$, root mean square error $\text{RMSE} = \sqrt{\frac{1}{N} \sum (O - M)^2}$, normalized bias $\frac{\sum (O - M)}{\sum O}$, normalized root mean square error $\text{NRMSE} = \frac{\sqrt{\sum (O - M)^2}}{\sqrt{\sum O^2}}$, and scatter index $\text{SI} = \sqrt{N^{-1} \sum (O - M) / (N^{-1} \sum O)}$, where N is the sample size.

3.1 Wave and circulation models

All model runs used a $0.5^\circ \times 0.5^\circ$ global grid, forced by hourly 0.20° wind fields and 6-hourly 0.5° ice concentration from the Climate Forecast System Reanalysis (CFSR) (Saha and et al 2010). The spectral space was discretized over 25 frequencies logarithmically spaced from 0.04 to 0.4 Hz and 24 directions (15° resolution). The source term parameterizations of Ardhuin et al. (2010) are used. This set of parameterizations describes the wind input term (S_{in}) adapted from Janssen (1991) with modifications by Bidlot et al. (2005) and the whitcapping dissipation term (S_{ds}) as a two-phase process represented by inherent breaking and a cumulative effect. A term for slow dissipation of non-breaking swell waves (S_{swell}) is included. The discrete interaction approximation (DIA) method (Hasselmann et al. 1985) is employed for computing the nonlinear wave–wave interactions (S_{nl}). Since topography-induced effects are irrelevant for the simulations, neither bottom friction nor triad interactions (relevant in shallow water) are considered.

For simulations in the presence of currents, the CFSR surface currents are also used. The current fields are represented by global regular grids of 0.5° resolution at provided every 6 h. For the additional simulation with high-resolution currents, the HYbrid Coordinate Ocean Model (HYCOM, details at <http://hycom.org>), represented by surface currents spatially spaced in $1/12^\circ$ cell nodes, is applied. The current fields are interpolated onto the 0.1°

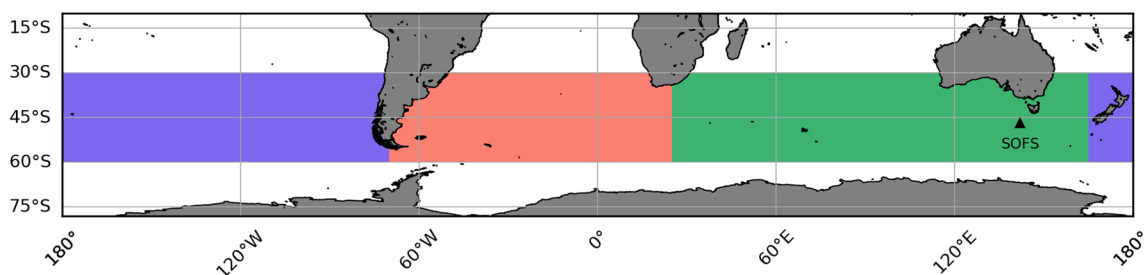


Fig. 1 Southern Ocean sectors used to validate the performance of the wave model: Atlantic (light red), Indian (green) and Pacific (blue). The location of the SOFS buoy is shown by the triangle mark

computational grid of dimensions 135–145° E and 52–45° S, which is nested to the coarse global grid. This domain is chosen in order to include relevant circulation features near the SOFS buoy. The grid is positioned with the SOFS buoy on its northwest corner so that the incoming west-southwest waves cross the finer grid area until they reach the buoy location. By doing so, we have the opportunity to qualitatively investigate the relevance of the current resolution to wave propagation and the refraction on mesoscale current features.

3.2 Observations

Spaceborn radar altimeters have been used for decades to determine wave height, with accuracy comparable to buoy observations (Caires and Sterl 2003). These data have been used by many studies to access wave model performance (e.g., Tolman 2002; Ardhuin et al. 2010; Durrant et al. 2013). The precise measurement of the distance of the satellite to the sea surface can provide the total variance φ^2 of the sea surface elevation, which is related to significant wave height as $H_s = 4\sqrt{\varphi^2}$. Although the altimeter validation is limited to wave height, it provides the valuable benefit of looking at a broad spatial scale with an extended database of more than 30 years. Despite the proven accuracy of altimeters, they do typically contain systematic biases (e.g., Cotton and Carter 1994; Durrant et al. 2009) that must be removed, especially when considering multiple instruments as is the case in this study. The data used here were obtained from the Globwave project, a quality-controlled, calibrated, and homogenized data set maintained at the French Research Institute for Exploitation of the Sea IFREMER (Queffeuilou and Croizé-fillon 2014). For the time frame of our analysis, data from the European Spatial Agency's (ESA) CryoSat and Envisat and the National Aeronautics and Space Administration's (NASA) Jason 1 and 2 were available.

The validation is also performed with in-situ data from the SOFS. The SOFS is part of the Australian Integrated Marine Observing System (IMOS, Meyers 2008) and was planned to provide a better understanding of the meteorological-oceanographic conditions in an area considered to play a key role in the global climate system. From the five deployments since 2010, we use in this study the second one (SOFS-2), which is justified by the presence of two wave sensors, the success in data acquisition, and the relative long time in which the buoy was operational (approximately 9 months). Two wave meters were installed: a motion reference unit (MRU) and a TriAxys directional wave sensor. Rapizo et al. (2015) compared the results from both sensors and showed that the TriAxys is more reliable based on the longer sampling time used in the spectral estimates and, consequently, higher confidence levels. We thus use only the

TriAxys output in our analysis. The inclusion of the SOFS in the analysis expands the investigation to the main wave parameters, in particular the peak and mean periods (T_p and T_{m01} , respectively) and directions (θ_p and θ_m), which are commonly used to describe the wave conditions. The SOFS was located at approximately 47°S and 142°E.

The deployment period of each sensor—satellites and buoy—and parameters used to validate the modeling results is given in Table 1.

4 Results

In this section, results of the simulations are analyzed, compared, and discussed. The simulations performed are as follows: (1) in the absence of currents; (2) in the presence of currents with the relative wind effect activated (RWND ON); (3) the same as (2) but with RWND deactivated (RWND OFF); and (4) in the presence of currents and with higher resolution computational grid (0.1°) and input current fields (1/12°). From the comparison of cases (2) and (3), we can quantitatively examine the relative importance of currents for wave generation and propagation. It should be stressed that simulation (4) is not validated; however, it provides an interesting discussion on how accurate the resolution of widely used hydrodynamic reanalysis can represent wave refraction and associated processes of convergence and divergence of wave energy.

4.1 Effects of currents on the spatial H_s field in the SO

The time averaged bias in H_s and RMSE against the altimeter data for the global simulations in the absence and presence of currents is shown in Fig. 2. Statistics are calculated for the period—Dec-2011 to Dec-2012—in $2^\circ \times 2^\circ$ bins. All altimeter missions shown in Table 1 are combined. The significant positive bias in the absence of currents at high southern latitudes reported in other studies (e.g., Ardhuin et al. 2010; Durrant et al. 2013; Zieger et al. 2015) is evident. The global H_s bias is 0.073 m with RMSE of 0.427 m, where the largest bias and error zone is found to be in the latitude range of 40°–60° S within which the SOFS buoy is located. It is possible to see from the visual analysis a considerable reduction of mean biases and errors of high southern latitudes in the simulation with currents (bottom panel). This result was also mentioned by Zieger et al. (2015) in their calibration of the source term parameterizations. A progressive decrease of errors is observed towards the upper latitude limit of 30°S, where the modeled energy is more accurate in the absence of currents and is not as affected by the current field.

It is worth noting the presence of local maxima of RMSE in the very high latitudes. These are due to the known impact

Table 1 Details of data sources used to validate the model results

Data source	Wave sensor (Mission)	Time frame	Analyzed parameters
Altimeter	Jason-1	Dec-2011 to Mar-2012	H_s
		May-2012 to Dec-2012	
	Jason-2	Dec-2011 to Dec-2012	H_s
	CryoSat	Jan-2012 to Dec-2012	H_s
	EnviSat	Dec-2011 to Apr-2012	H_s
Buoy	TriAxys	Dec-2011 to Jul-2012	H_s , T_p , T_{m01} , θ_p and θ_m

of wave energy blocking by floating icebergs (Ardhuin et al. 2011), an effect not accounted for here. Since our simulations do not include icebergs, these local errors are ignored to avoid uncertainty in the assessment of the relative impact of currents on the wave field.

Figure 3 shows the scatter density plots of both simulations, with and without the presence of current fields. The analysis is separated by major oceans—Atlantic, Indian, and Pacific—and also performed for the whole SO area (top to bottom panel rows, respectively). Statistical parameters are shown in each panel. Absolute bias of 0.32 m and RMSE of 0.56 m are observed in the absence of currents when considering the entire SO. The sector with larger bias and error is the Indian Ocean (panels b), followed by the Pacific (c) and Atlantic (a) Oceans. When currents are included in the simulation, the reduction of the mean bias is of 8 cm and RMSE is improved by 6 cm for the SO. The reduction of bias is more prominent for the sectors where bias is larger, i.e., in descending order Indian, Atlantic, and Pacific Oceans for which biases decrease in 0.087, 0.07, and 0.064 cm, respectively. The zone of highest bias is found in the range (40° – 60° S). The absolute and normalized

statistical measures for all sectors and for the whole SO area are shown in Table 2.

The reduction of overall bias in H_s in the SO can be better visualized through the quantile–quantile plots (up to the 99th percentile) of model against data for simulations without and with currents (Fig. 4). As shown in Fig. 3, the inclusion of currents (right panel) reduces the overestimation of wave height observed in the absence of current forcing (left panel). The reduction is more accentuated for larger waves.

There are several likely reasons for the improved statistics of modeled wave height in the presence of currents, firstly, the impact of the ACC in weakening the effective wind since winds and waves have a similar resultant direction. The predominance of westerly winds and of a geostrophic eastward ocean flow results in a configuration of wave growth over co-flowing currents. If the effective wind is reduced, which in the model is represented by a simple balance between wind and current vectors, and the amount of energy from the wind input decreases (see Section 2). The ACC velocity axis is positioned in the 40 – 60° S zone as observed from the CFSR reanalysis. Figure 5

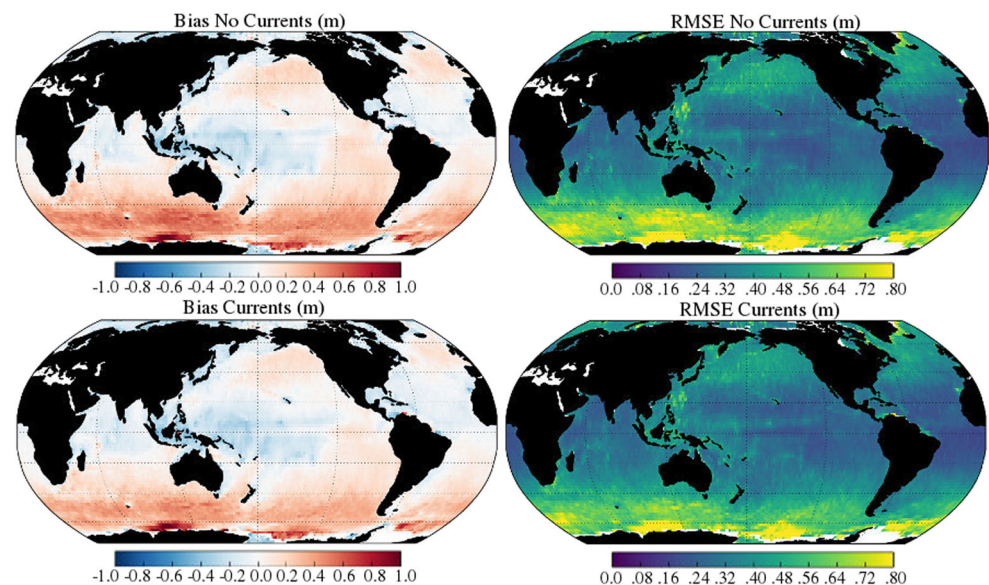
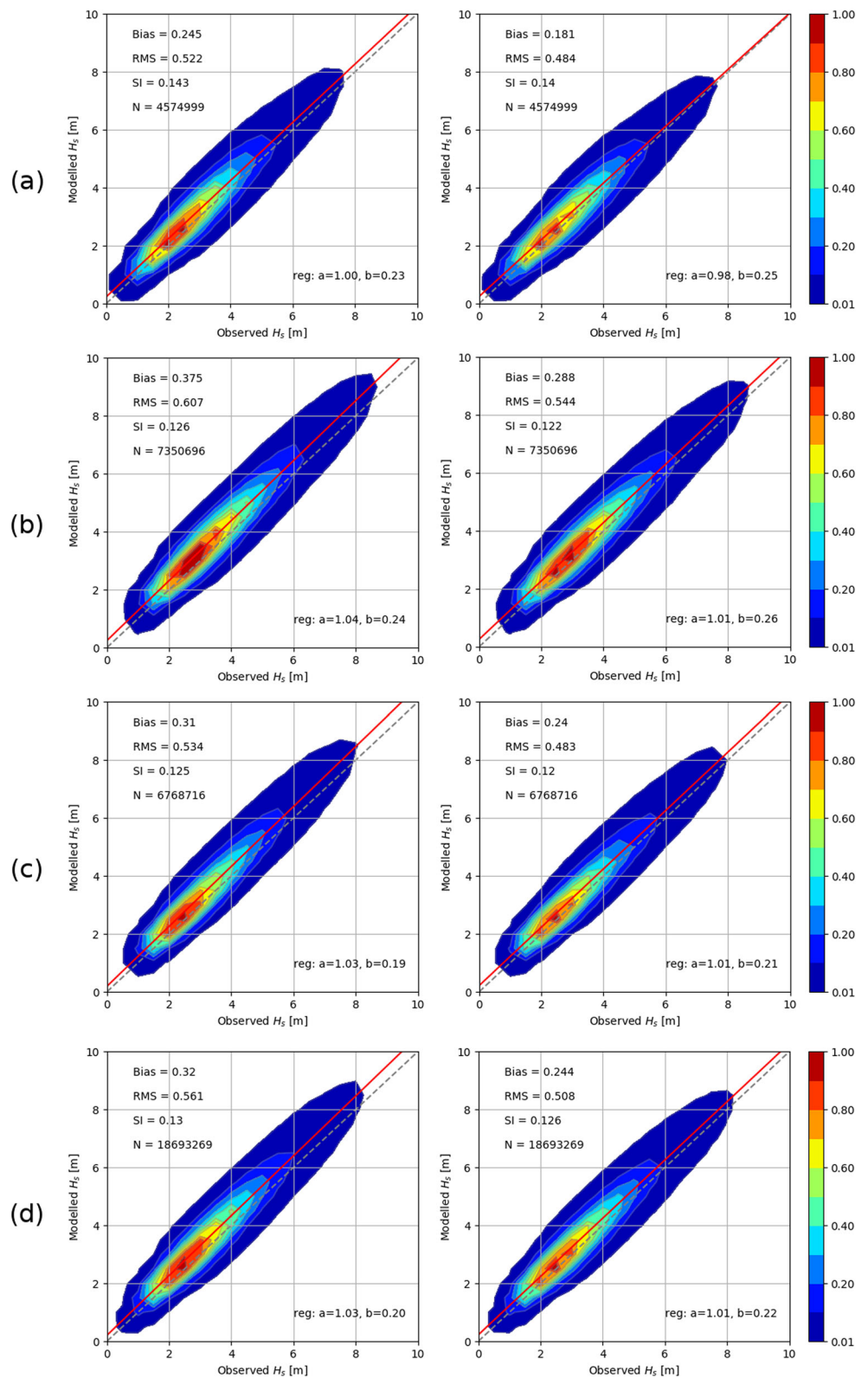
Fig. 2 Global distribution of significant wave height bias (left panels) and RMSE (right panels) for simulations in the absence (top panels) and presence of currents with RWND ON (bottom panels)

Fig. 3 Scatter density plots for the SO. Results for the simulations in the absence (left) and presence (right panels) of currents are shown, separated by SO sectors: **a** Atlantic; **b** Indian; **c** Pacific; and **d** all. Statistical parameters of bias, root mean square error (RMSE), scatter index (SI), and number of samples (N) are given for each plot. Reference line (dashed) and best-fit line (red) are depicted in each plot, for which parameters of slope and intercept (a and b , respectively) are shown in the lower right corner of each plot



shows the mean velocity field at 5-m depth for July-2012. The eastward flow associated with the ACC is clearly visible in the latitude range where the reductions in bias and error

in wave height are more accentuated (Fig. 2). Larger mean current speed with a more defined east flow is observed in the Indian sector, followed by the Pacific and Atlantic

Table 2 Validation of modeled H_s against altimetry data for the Southern Ocean sectors: Atlantic, Indian, Pacific, and all

SO sectors	N	Bias (m)	NBias (%)	RMSE (m)	NRMSE (%)	SI
Atlantic	4574999	0.2452	7.629	0.5219	16.236	0.1433
Atlantic (C)	4574999	0.1810	5.631	0.4842	15.063	0.1397
Indian	7350696	0.3753	9.904	0.6071	16.022	0.1259
Indian (C)	7350696	0.2877	7.591	0.5439	14.352	0.1218
Pacific	6768716	0.3099	8.896	0.5340	15.330	0.1249
Pacific (C)	6768716	0.2399	6.886	0.4832	13.871	0.1204
All	18693269	0.3198	9.039	0.5611	15.860	0.1303
All (C)	18693269	0.2443	6.904	0.5082	14.363	0.1259

Statistical quantities are represented by: number of samples (N), absolute bias, normalized bias N Bias, root mean squared error (RMSE), normalized root mean square error (NRMSE), and scatter index (SI). The letter C within parenthesis corresponds to simulation with currents

sectors (except for the strong jet past the Drake Passage), which are respectively the sectors with larger improvements in modeled wave height.

Another possible effect is the reduction of energy due to the decrease (increase) in wavenumber (wavelength). The co-flowing current lengthens the waves compared to waves propagating on quiescent water (Longuet-Higgins and Stewart 1961). This leads to a reduction in wave energy due to the conservation of wave action $E/\sigma(k)$ (e.g., Bretherton and Garret 1969). The currents can also modify the wave velocity. If waves are still receiving energy from the wind but start propagating faster due to the moving medium, they will propagate out of the area of wind influence faster than expected in the case without currents (e.g., Peregrine 1976). This would have an impact on the time and length scale of the generation process. The duration of wave growth would shorten and the effective fetch on which the waves grow would be reduced. Furthermore, refraction induced by current gradients can create zones of convergence (increase)

and divergence (decrease) of wave energy. All these effects are accounted for in the wave model.

The aforementioned effects (generation and propagation) can be quantified by activating and deactivating the relative wind in the model. The differences in the time averaged H_s between currents and no-currents simulations ($\Delta H = H_{s\text{Curr}} - H_{s\text{NoCurr}}$) are shown in Fig. 6. With RWND activated (top panel), strong differences are apparent. When RWND is deactivated (bottom panel), the wind input quantity is unchanged and the current-induced effects on propagation are not strong enough to impact the mean H_s field, except for some mesoscale features that will be discussed later in this section. This suggests that the reduction of the mean wave energy (thus the reduction of the overall positive bias) observed in the presence of currents is predominantly due to the relative wind effect in a global scale, except where strong local currents occur. A strong effect is seen in the SO, indicating that the Antarctic Circumpolar Current (ACC) plays a key role in reducing the

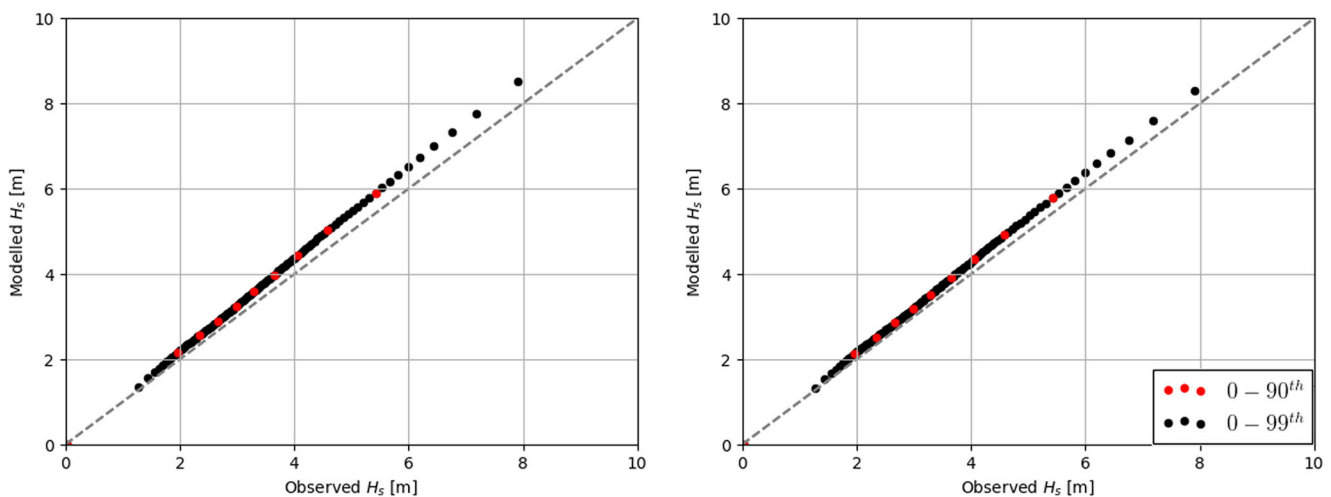


Fig. 4 Quantile–quantile plots for simulations in the absence (left) and presence (right panel) of currents. Red markers show values up to the 90th percentile and black markers up to the 99th percentile

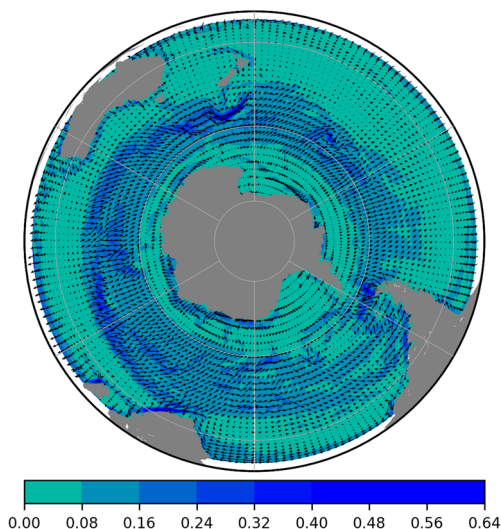


Fig. 5 Mean current field in the SO for July-2012. Color scale represents current speed in m/s

momentum transfer from the wind to the waves. It should be noted that Saha and et al (2010) found that the CFSR current reanalysis underestimates the ACC magnitude, and therefore the wave height bias reduction observed in this study is likely underestimated. It is worth mentioning that current meters were deployed in the SOFS mooring cable.

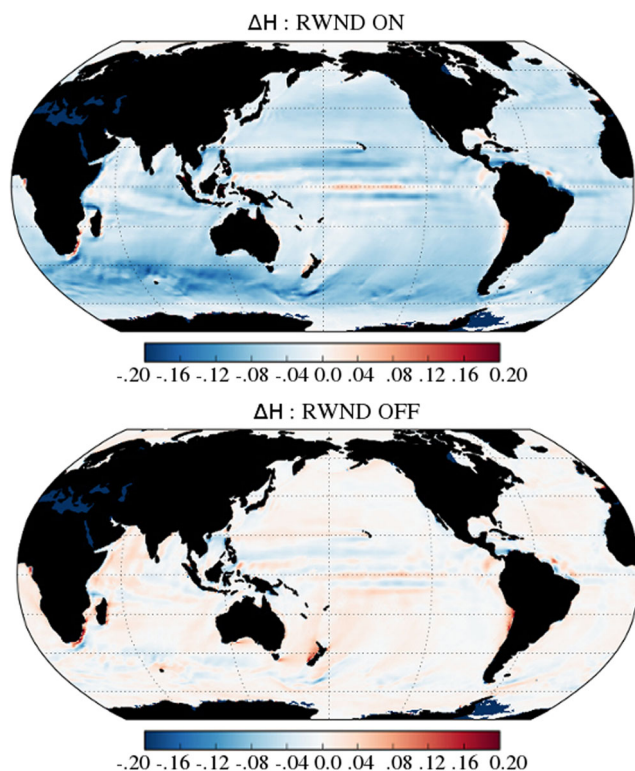


Fig. 6 Difference between H_s fields for the simulations with and without currents ($\Delta H = H_{sCurr} - H_{sNoCurr}$). The top and bottom panels show results for RWND activated and deactivated, respectively

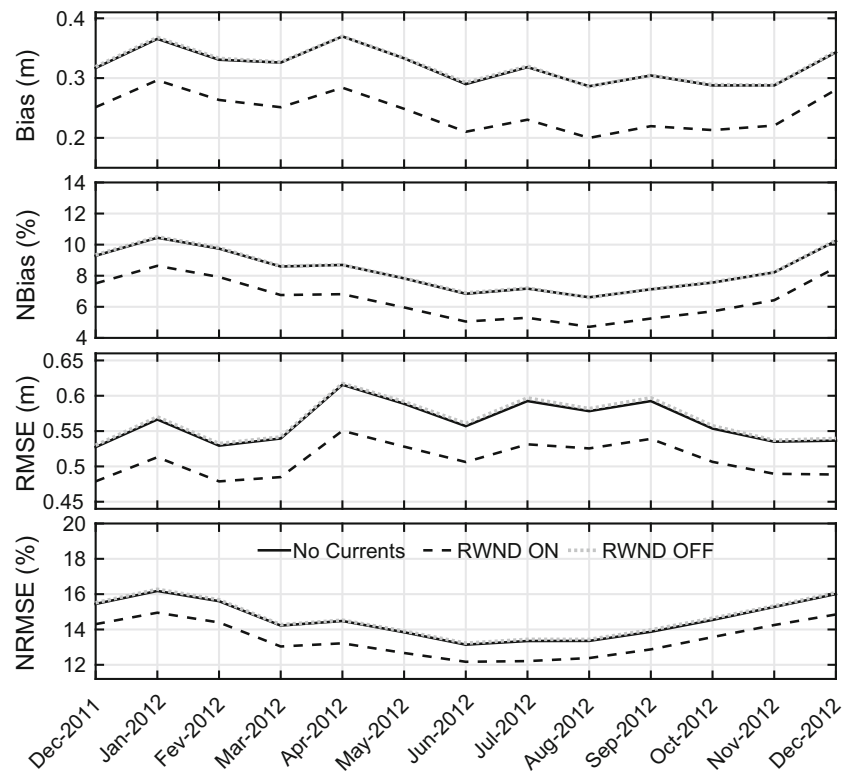
These data need to be analyzed and will be used in a future study to assess the accuracy of the CFSR currents at these Southern latitudes.

Although the overall changes in wave height are strongly associated with the relative wind, some notable mesoscale features can be noticed in the lower panel of Fig. 6 (RWND OFF). Marked positive values of ΔH over the Agulhas current are unchanged when RWND is not considered indicating that changes in the wave energy distribution in this region are mostly related to propagation, refraction, and energy convergence due to the opposing flow. Alternating patterns of positive and negative values can also be observed on the equator caused by co-flowing and opposing flows of the equatorial current and counter-current. And also an alternating color pattern is seen on the Drake Passage, where the jet flow likely produces convergence and divergence of wave energy. The downward flow from the South Pacific gyre and East Australian Current generates positive ΔH values around the New Zealand islands and east of Tasmania. Other mesoscale features exclusively associated with propagation effects include the Indonesian Throughflow, the North Brazilian Current, and the circulation in the South China Sea and Luzon Strait. All these mesoscale features modify the wave height and have a potential impact on the wave climate.

The absolute and normalized statistical parameters in the absence and presence of currents are analyzed by means of their monthly mean values in Fig. 7. The values correspond to the entire SO area, where results for all satellite missions were averaged. Results for the “RWND ON” (effective wind activated) and “RWND OFF” (relative wind deactivated) regimes are plotted with different line styles (black dashed and grey dotted lines, respectively). Despite the non-patterned behavior of the absolute quantities, the normalized statistics show lower bias and errors during the austral winter months with a progressive increase towards the summer of 2012. Since the absolute bias and error do not show any clear variation over the 13 months, the normalized errors decrease in winter since the mean wave height is higher during this period compared to summer in the SO (e.g., Rapizo et al. 2015). The analysis of Fig. 7 shows that the currents affect the mean modeled wave height in the SO mostly when the relative wind is activated (“RWND ON”), with the exception of localized areas of strong current jets, as previously discussed. When RWND is not considered (dotted lines in the plots of Fig. 7), the differences in the average monthly statistics are practically imperceptible and the errors actually increase slightly in some months.

The statistical parameters in Figs. 6 and 7 correspond to yearly and monthly averaged values, respectively. The investigation of the separated effects of currents on wave generation and propagation becomes more interesting when a snapshot of the results from the “RWND ON” and

Fig. 7 Monthly mean statistics of the modeled H_s in the SO. Panels from bottom to top show: normalized root mean square error (NRMSE), absolute root mean square error (RMSE), normalized bias (NBias), and absolute bias. Definition of all statistical variables used is given in Section 3



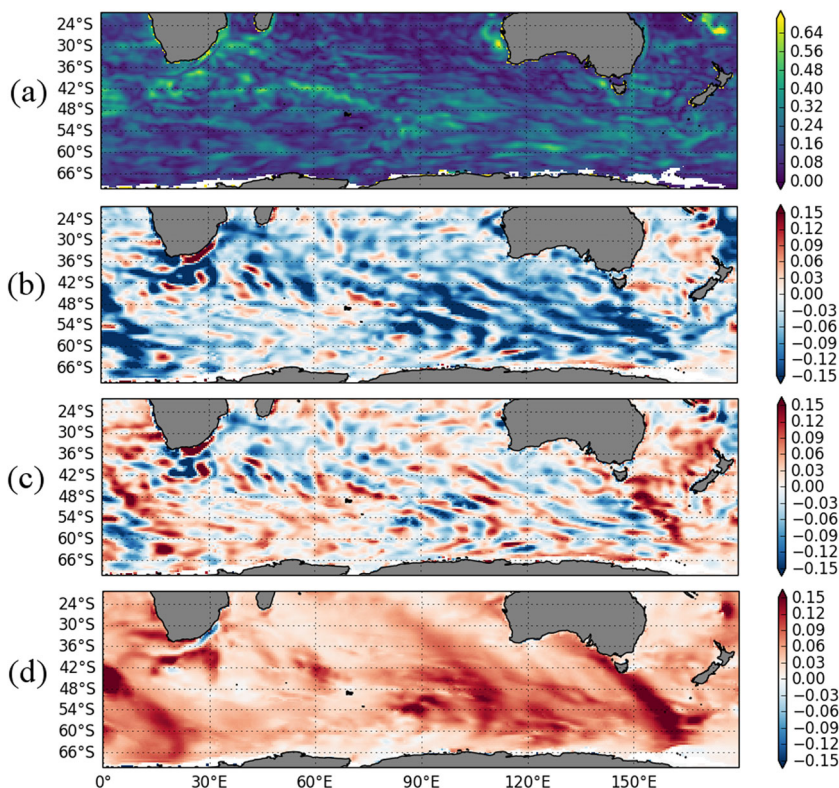
“RWND OFF” simulations are analyzed. Figure 8 shows the effects of the spatial distribution of currents on the wave field in the SO for a selected time step. Note that this domain is not the same domain of the SO used in the statistical analysis. We chose an arbitrary region to exemplify the effects observed. The distribution of current speed is shown on panel (a), followed by (from top to bottom) ΔH fields for simulations using “RWND ON” and “RWND OFF” (panels (b) and (c), respectively). The last panel (d) shows the difference between plots (c) and (b) (“RWND ON” and “RWND OFF”). The distribution of ΔH values reveals an interesting spatial pattern of crests and troughs that propagate in the direction of the wave fronts. These patterns are clearly modulated by the spatial distribution of the currents. However, the magnitude of ΔH is considerably different in cases (b) and (c). For “RWND ON,” the current field predominantly reduces the relative wind speed, which results in lower wave heights (see Section 2), creating negative values of ΔH . A spatial pattern of alternate values of negative (blue) and null (white) values is created. On the other hand, in the “RWND OFF” case, the difference ΔH increases and the oscillations are represented by alternating positive (red) and negative values.

The difference between the two simulations can be explained by the balance between the current effects on wave generation and propagation. When RWND is deactivated, the momentum flux from wind to wave is unaltered. Thus, the wave growth has the same intensity as in the absence of

currents, consequently resulting in the same wave energy generated. However, waves run on average faster throughout the Southern Ocean area. This is because the absolute group velocity $\mathbf{C}_g = \mathbf{c}_g + \mathbf{U}$ is increased since waves and currents have the same mean direction (from west/southwest) (see Eq. 1 in Section 2). It should be remembered that the term \mathbf{C}_g is responsible for transporting the wave energy in geographical space (see Eq. 1). In deep water, the magnitude of the intrinsic group velocity is $c_g = c_p/2$, where the phase velocity is c_p , and it has same direction as the wavenumber vector. Therefore, with no relative wind effect (i.e., $a = 0$ in Eq. 2), waves are modulated along their propagation by the distribution of currents through the modification of \mathbf{C}_g . Wave refraction induced by current gradients and consequent convergence and divergence of energy play a small role in our simulations, which may be an artifact of the coarser numerical grid (discussions in Section 4.3). The correlation of the spatial distribution of wave height with mesoscale current features was recently shown by Arduin et al. (2017). The current field used in their study was capable of reproducing mesoscale vortices well. As we shall see in Section 4.3, however, the current field provided by commonly used global reanalysis and applied in our study is not resolved enough in its spatial distribution and wave refraction is poorly simulated.

Because the average wave and current directions are very close in the Southern Ocean, the generated swells run faster compared to simulations in absence of currents for RWND

Fig. 8 Spatial effects of current on the wave field for a selected time step (2012-02-11T03:00): (a) current speed (m s^{-1}), (b) $\Delta H = H_{s\text{Curr}} - H_{s\text{NoCurr}}$ for RWND activated, (c) RWND deactivated, and (d) the H_s difference between simulations using RWND OFF and ON (in meters).



ON. This process creates a time lag in the propagation of wave fronts and contributes to the positive values (red) of $\Delta H = H_{s\text{Curr}} - H_{s\text{NoCurr}}$ observed in Fig. 8c. In the case of “RWND ON” (panel (b)), the momentum flux from wind to the waves is decreased due to following currents. The generated waves have less energy and lower periods and, as a consequence, negative values (blue colour) of ΔH predominate.

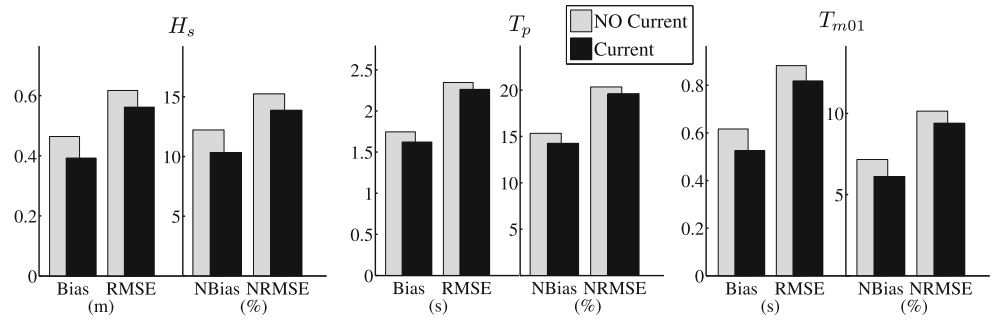
4.2 Validation against the SOFS buoy

In this section, in situ measurements from the SOFS directional wave buoy are used to estimate the influence of ocean currents on wave modeling in the Southern Ocean. We should be careful in the interpretation of the results since the validation of one point only may not be representative of the entire SO. The SOFS buoy however lies within the range of the largest wave height bias observed (40°–60° S) and it offers a valuable opportunity of validating the WW3 performance at high southern latitudes. The parameters of H_s , T_p , T_{m01} , θ_p , and θ_m are analyzed. For a detailed description of the characteristics of the wave sensor and the spectral estimation method applied, the reader is referred to Rapizo et al. (2015). When current forcing is included, the observed reduction of bias for the modeled wave height seen against altimetry data is also observed for H_s , T_p , and T_{m01} using the SOFS data. Figure 9 shows the histogram comparison between current and no-current simulations.

The improvements for the run with current are observed for all absolute and normalized statistics. The magnitude of the differences is similar to the improvements observed for the validation against altimeters. For the SOFS, the differences in absolute and normalized biases are 0.0722 and 0.0189, respectively, whereas for altimeter (considering the entire SO), they are 0.0755 and 0.0213.

Overall improvements are observed in the simulation of all wave parameters. To complement this analysis, we compare the normalized bias difference between the simulations with and without currents, i.e., $\Delta \text{NBias} = \text{NBias}_{\text{Curr}} - \text{NBias}_{\text{NoCurr}}$, as functions of the modeled H_s and T_p in the absence of currents (Fig. 10). This analysis shows the waves that are more affected by the current field. The mean period exhibits a very similar behavior to the peak period and is not shown here. The values were placed in seven bins between the minimum and maximum value of each range as indicated in Fig. 10. The total number of 3049 records is analyzed. Although this number is not as large as it is for altimeters, the distribution of samples exhibit the known Rayleigh-type and normal-type shapes for H_s and T_p , respectively. The NBias difference increases towards higher (top left panel) and longer (top right panel) waves. This result suggests that the inclusion of currents affects distant-generated swells more than local seas at the SOFS location. Rapizo et al. (2015) found a strong predominance of swell for the measured waves at the SOFS, with swell fraction of ~ 0.8 . Due to practically unlimited fetches

Fig. 9 Histogram plots of the model performance between simulations in the absence and presence of currents for the wave parameters H_s , T_p and T_{m01}



and persistent strong winds, these SO swells are generated over a large area and long periods of time. Hence, this relative reduction in wind input in the presence of currents has a cumulative effect on the swell systems, resulting in a relatively larger effect on swells than on locally generated seas. However, we must consider that in our simulations, the reanalysis current fields have low resolution and cannot describe well local mesoscale features (discussion in Section 4.3). Thus, the current-induced modulation of local seas is not as well represented as the large scale effects on swell.

Table 3 contains the results of the model performance for all wave parameters. Only the normalized statistics are shown for wave height and period. The statistical variables for validating the peak and mean directions are represented by the root mean square ϵ_{rms} and standard deviation ϵ_σ of the angle difference between the modeled and observed vectors. Differently from the one-dimensional spectral parameters, the directional standard deviations and errors are not improved much and the mean direction statistics slightly deteriorate. This result indicates that wave propagation and refraction on the current field have little effect on the mean directional properties of waves, which is probably a limitation of the coarse current resolution. These limitations are discussed in the next section.

4.3 On the importance of the current grid resolution

The inclusion of currents improves the model results for all parameters except for the wave direction. The improvements of modeled wave height are closely related to changes in the relative wind speed, whereas the propagation effects seem to be negligible for the mean statistics, except in areas of strong/localized currents such as the Drake Passage and the Agulhas Currents. The impact of the current field on wave propagation and, more specifically, on the wavenumber and direction is associated with the horizontal gradients of the current field, which requires a reasonably accurate spatial resolution in order to represent mesoscale oceanic features such as geostrophic vortices. Therefore, it is important to understand the capability of global wave models in simulating wave refraction properly. Widely used reanalysis products provide horizontal currents in grid resolutions usually in the range $0.5^\circ-1^\circ$.

In this section, the importance of the choice of current grid resolution is investigated. Firstly, we briefly analyze how different spatial resolutions can influence wave refraction on typical mesoscale vortices. To do that, we revisit the classical example of wave propagation over a current eddy (e.g., Kenyon 1971; Mathiesen 1987) by numerically simulating the wave ray trajectories induced

Fig. 10 Difference of normalized bias $\Delta\text{NBias} = \text{NBias}_{\text{Curr}} - \text{NBias}_{\text{NoCurr}}$ (top panels) between current and no-current simulation and number of samples (bottom panels) as functions of modeled H_s (left) and T_p (right) in the absence of currents

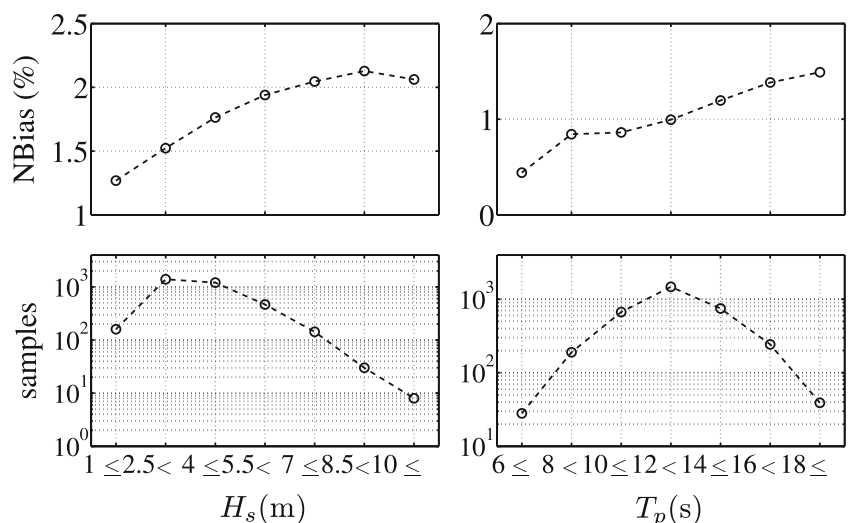


Table 3 Validation of the model against the SOFS data for all analyzed parameters (H_s , T_p , T_{m01} , θ_p , and θ_m)

	H_s		T_p		T_{m01}		θ_p		θ_m	
	NB (%)	NRMSE	NB (%)	NRMSE	NB (%)	NRMSE	ϵ_σ (deg)	ϵ_{rms}	ϵ_σ (deg)	ϵ_{rms}
No currents	12.2	15.2	15.4	20.5	7.2	10.1	20.9	30.6	15.6	25.0
Currents	10.3	13.9	14.4	19.7	6.1	9.4	20.8	30.5	15.7	25.2
Improvement (%)	15.5	9.0	7.0	3.5	14.7	7.2	0.4	0.35	-0.6	-0.7

Statistical quantities are represented by normalized bias (NB), normalized root mean square error (NRMSE) (for one-dimensional parameters) and root mean square error (ϵ_{rms}), and standard deviation (ϵ_σ) of the angle difference (for directional parameters). Improvements of the modeled parameters in the presence of currents are shown in the last row, where negative values represent deterioration of statistics

by changes in wavenumber and direction. The idealized eddy model used in Mathiesen (1987) is applied with a maximum current speed of 1 m s^{-1} and radius of 1.5° ($\sim 166.5 \text{ km}$). The velocity transect is represented by a tangential velocity that increases linearly from the center to the point of maximum speed and a Gaussian profile further away from this point. The dimension and magnitude were chosen to represent similar features to those observed in the Southern Ocean from the HYCOM reanalysis. The refraction of a wave train with $T = 12 \text{ s}$ (the mean T_p value at the SOFS found in Rapizo et al. 2015) is examined for various spatial resolutions of the current field: 0.5° ($\sim 55.5 \text{ km}$), 0.25° ($\sim 27.75 \text{ km}$), and 0.1° ($\sim 11.1 \text{ km}$) (Fig. 11).

As the resolution decreases, the refraction and related processes of convergence and divergence are poorly represented. The spatial resolution of 0.5° (right panel of Fig. 11) equivalent to the CFSR current grid used is considerably less accurate than the highest resolution (0.1°) in solving refraction induced by eddies of such a length scale.

In order to demonstrate the impact of a high-resolution current on wave modeling more clearly, an additional simulation using the WW3 model is performed. This last test is for a qualitative assessment only and performed over a short period of time (1 month). A high-resolution current grid in the range $135\text{--}145^\circ \text{ E}$ and $45\text{--}52^\circ \text{ S}$ ($7^\circ \times 10^\circ$) is nested to the global grid. For this finer grid, the current fields are provided by the HYCOM + NCODA Global Reanalysis (<http://hycom.org/data/glb0pt08/expt-19pt1>) with $1/12^\circ$ spatial resolution twice daily. The spatial

resolution is thus more detailed than in the idealized model used in the left panel of Fig. 11 and hence is capable of representing wave refraction on mesoscale eddies. The domain of the high-resolution current grid is selected in order to include possible ocean eddies and to allow the model to properly represent the refraction of the incoming waves.

We could observe several eddies in the HYCOM currents that are formed near the SOFS buoy. These eddies can keep their approximate position for days and may consistently affect the waves that propagate over this region. Figure 12 shows an example of the formation of a relatively strong eddy ($\sim 1 \text{ m/s}$) and its effects on the wave height distribution within the grid area. Four time snapshots separated by an interval of 3 days and 21 hours are shown. The top panels (a) show the current speed predicted by the high-resolution reanalysis, where we can clearly identify the eddy, which dimension and intensity are very similar to those given by the theoretical model used in Fig. 11. The wave height difference ΔH between the current and no-current simulations is shown in the middle (b) and bottom (c) panels, respectively. In (b), the high-resolution grid with the HYCOM currents is used. Panels (c) show results for the CFSR currents only. The results of both simulations are compared in the global output grid (0.5°). The patterns of convergence and divergence are considerably better defined for the nested simulation (b). An alternating pattern of positive (energy convergence) and negative (divergence) ΔH values is evident in the right panel of row (b). This pattern is typical of the eddy-induced wave refraction (e.g.,

Fig. 11 Wave rays refraction on a theoretical eddy. Three different spatial resolutions of the eddy are shown (from left to right): 0.1° , 0.25° , and 0.5°

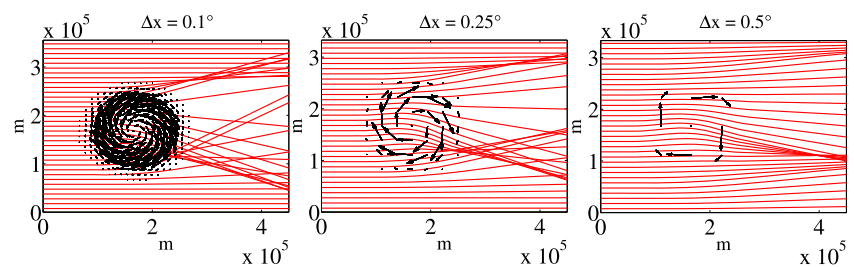
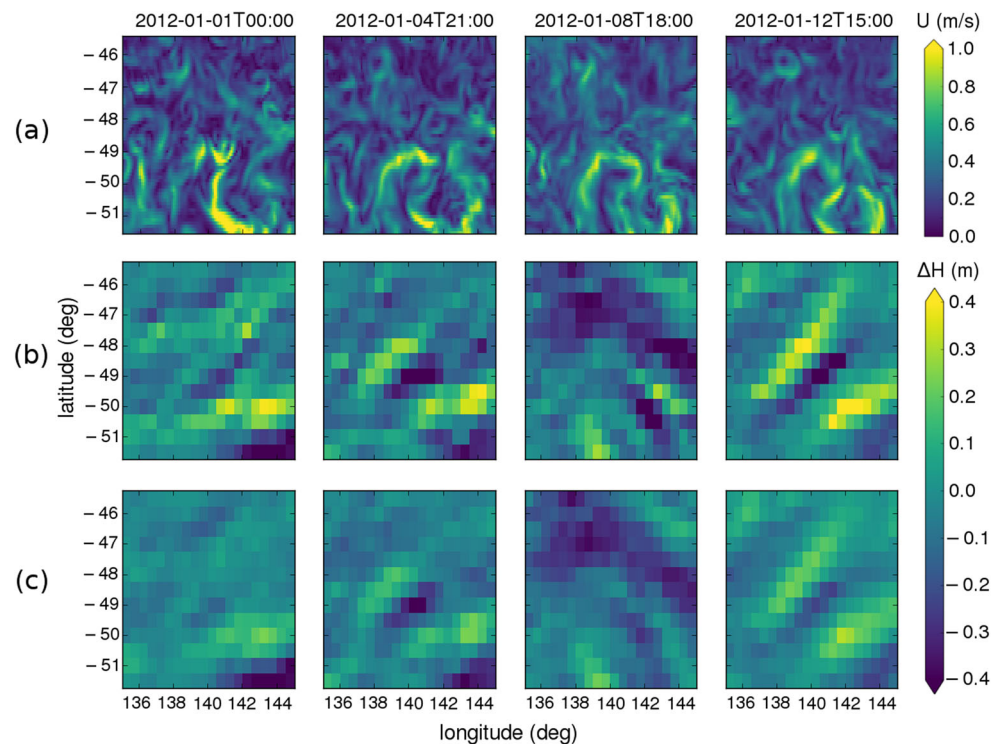


Fig. 12 Current speed and ΔH in the domain used for the high-resolution grid at four different moments. Panels (a) show current speed from the HYCOM reanalysis. The results for ΔH are shown for the simulations with current, (b) for global CFSR currents nested to the high-resolution HYCOM currents, and (c) for global CFSR currents only



Mathiesen 1987; Rapizo et al. 2014). When only the global currents are applied, the refraction-induced ΔH patterns are poorly represented.

The results of Fig. 12 together with the patterns of wave ray refraction for different spatial resolutions of the current field (Fig. 11) indicate that typical resolutions of widely used global reanalysis are not sufficient for resolving ocean eddies and, consequently, wave refraction. Therefore, the distribution of modeled wave height as well as other wave parameters can be compromised. The simulations used to assess the impact of currents on waves shown throughout Section 4 are based on current fields with 0.5° resolution, and therefore eddies and other mesoscale features are smoothed out. Consequently, the observed reduction of wave height bias reflects mostly the importance of the large-scale relative wind effect. The recent study from Ardhuin et al. (2017) showed that mesoscale currents can be significant in modulating wave height due to refraction; however, the resolution of the current-field reanalysis used in our simulations does not allow to estimate the importance of refraction on mesoscale and on the large-scale bias in the SO.

5 Accuracy of wind and current models

The discussion on the relevance of currents to the Southern Ocean wave field is incomplete without an assessment of the accuracy of the forcing fields. The observed wave patterns

are primarily a result of the wind distribution and, as discussed, are modified by the presence of surface currents. In the SO, our results showed that the co-flowing currents decrease the wave energy mostly because of an overall reduction in the relative wind. However, a considerable positive bias remains (Section 4). It is not clear from the results of the previous sections whether the presence of this remaining bias is associated with wave model physics, due to the poor resolution of wind and current grid as shown in Section 4.3 or simply transferred to the wave model by inaccurate forcing. A quantitative assessment of the impact of currents on wave refraction is not possible with the spatial resolution provided by the CFSR as seen in Figs. 11 and 12. Nevertheless, we can verify if part of the large-scale bias is directly passed on to the wave model by wind and current forcing.

The validation of the wind speed provided by the CFSR against satellite data for the SO is shown in Fig. 13. The modeled winds, which have mean direction close to wave propagation (west/southwest), show a very similar pattern of positive bias in the latitude range considered (30° – 60°). Similar results were reported in Chawla et al. (2013) and Stopa and Cheung (2014). It indicates the H_s bias shown in this and other studies are partially associated with a positive bias in the wind product from the CFSR used to force the wave model.

In this study, we do not validate the current fields from the CFSR. However, it is worth discussing the results from Saha and et al (2010). The authors compared the

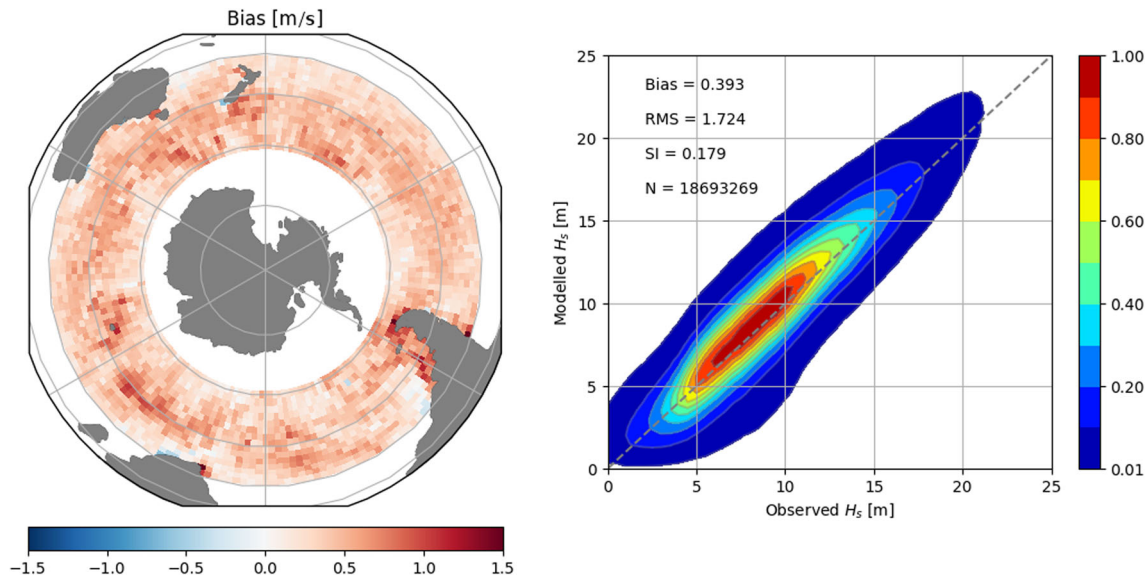


Fig. 13 Spatial distribution of absolute bias for CFSR wind speed for the year 2012 in the Southern Ocean (left) and associated scatter density plot. Displayed statistics are as in Fig. 3

reanalysis currents to surface drifters drogued at 15-m depth. The CFSR maps were compared to the current fields derived from the pseudo-Lagrangian motion of drifters. The modeled currents show good agreement to measurements in the Northern Hemisphere and in the tropical range but have a smaller eastward velocities in the Southern Ocean, specially in the latitudes 40°–60°. The ACC was seen to be a key component in reducing the momentum flux from wind to waves. Therefore, its underestimation in the reanalysis used hinders a complete representation of the role of currents in decreasing the wave height in the SO. A proper representation of the current field in the Southern Hemisphere will thus reduce the positive bias in H_s further. Furthermore, the CFSR poor resolution hinders a proper evaluation of propagation effects on the large-scale biases.

6 Conclusions

The relevance of ocean currents to wave modeling in large ocean basins is investigated. The approach taken consists of simulating wave fields using the WW3 model with and without surface currents. Some specific model settings are also modified to understand the cause of the observed differences, mainly by dividing the possible current-induced effects into wave generation and propagation. The results are validated against global altimetry data with the emphasis on the Southern Ocean and the wave parameters obtained from the analysis of the Southern Ocean Flux Station (SOFS). For the spatial validation of model results against altimeters, we divide the SO into three sectors: Atlantic, Pacific, and Indian Oceans.

In the absence of currents, the validation of the significant wave height H_s against altimeters shows positive biases and errors in high southern latitudes. The Indian Ocean sector has the highest bias (0.375 m) and RMSE (0.607 m), followed by the Pacific (0.310 and 0.534) and Atlantic (0.245 and 0.522) sectors, while for the entire SO, the values are 0.320 and 0.561, respectively. Biases are also observed when validating the model for H_s (0.466 m), T_p (1.762 s), and the T_{m01} (0.618 s) at the SOFS location. For the directional wave parameters, the validation shows standard deviation and root mean square error of the angle differences of 20.87 and 30.65 for θ_p and 15.60 and 25.03 for θ_m , respectively.

When surface currents are included in the model, a substantial improvement is observed for the simulation of the main wave parameters. The bias in the SO is reduced from 0.320 to 0.244 m and RMSE improves by 0.053 m, from 0.561 to 0.508 m. The sectors with largest biases and errors are also the ones with greater improvements of absolute and normalized statistics. In order to understand which mechanism is mainly responsible for the model improvements in the presence of currents, an additional simulation is performed without considering the relative wind (i.e., the vector balance between wind and current). By doing so, the momentum transfer from wind to waves is unaltered. Interestingly, from our analysis, the current-induced reduction of wave height is mostly related to the effective wind in the SO. Propagation effects play a smaller role in the overall mean reduction of H_s when using the CFSR currents. However, they are important in regions of relatively strong currents such as the Agulhas Current, in the Drake Passage and around the New Zealand islands. These

differences can potentially impact the wave climate in these areas. However, the small role of refraction on the reduction of large-scale biases is possibly a result of the low resolution of current fields provided by CFSR. Local structures are crucial to governing mesoscale spatial variations of H_s as shown in Ardhuin et al. (2017).

The current field improves the statistics for all non-directional parameters— H_s , T_p , T_{m01} —at the SOFS. For H_s , the normalized bias in the presence of currents is 15.57% of the value in the absence of currents, whereas for mean period, it is 14.70%. The peak period T_p is less sensitive to the inclusion of currents and Nb is 7.00% lower than that for no-current conditions. The analysis of the bias difference ΔNBias between simulations in the absence and presence of currents as functions of H_s and T_p shows that the currents have a stronger impact on larger and longer waves. Acknowledging that the effective wind is an important factor for wave height (and period) reduction, this result suggests that distantly generated swells are strongly affected and, at least from our simulations using CFSR currents, more affected than locally generated waves. However, it is necessary to bear in mind that the resolution of the current field hinders a proper description of mesoscale eddies and other features near the SOFS buoys.

Differently from the wave parameters discussed above, the modeled peak direction θ_p and the mean direction θ_m do not show noticeable improvements when currents are considered. In fact, mean direction statistics deteriorate. Although our results indicate that the one of the dominant mechanisms of wave height reduction is the decrease of relative winds, the less sensitivity of wave direction to the inclusion of currents can be an artifact of the coarse numerical and current grid resolutions. The numerical simulation of ray trajectories on a theoretical eddy shows that as the resolution decreases from 0.1° to 0.5° , the refraction of wave rays and associated patterns of convergence and divergence becomes inaccurate. Therefore, the spatial resolution of the current field must be such that ocean eddies are resolved so that they can reproduce modifications of the wave propagation path. As a qualitative test, we nested the global model to a high-resolution current grid with boundaries at $135\text{--}145^\circ\text{E}$ and $52\text{--}45^\circ\text{S}$ ($10^\circ \times 7^\circ$). The current field in this grid has high resolution ($1/12^\circ$). The visual comparison of the wave height in this domain shows that the presence of eddies can modify the wave height distribution and the definition of zones of convergence and divergence of wave energy. However, this result is a qualitative assessment only. Further investigation is planned to validate the simulations with high-resolution numerical and current global grids.

Acknowledgements We would like to thank Dr. Qingxiang Liu for valuable discussions on the modeling results. We are thankful to the anonymous reviewers for all suggestions and criticisms.

Funding information Buoy data were sourced from the Integrated Marine Observing System (IMOS)—IMOS is a national collaborative research infrastructure, supported by Australian Government. Support from the Australian Victorian Government through the Victorian International Research Scholarship and from the Australia-China Joint Research Centre for Maritime Engineering is acknowledged by the first author. A.V. thanks support from the Australian Research Council through Discovery Grant DP130100227.

References

- Alves JHGM (2006) Numerical modeling of ocean swell contributions to the global wind-wave climate. *Ocean Model* 11:98–122. <https://doi.org/10.1016/j.ocemod.2004.11.007>
- Ardhuin F, Rogers E, Babanin AV, Filipot J, Magne R, Roland A, Van der Westhuysen AJ, Queffelec P, Lefevre J, Aouf L, Collard F (2010) Semiempirical dissipation source functions for ocean waves. part i: definition, calibration, and validation. *J Phys Oceanogr* 40:1917–1941. <https://doi.org/10.1175/2010JPO4324.1>
- Ardhuin F, Tournadre J, Queffelec P, Girard-Ardhuin F, Collard F (2011) Observation and parameterization of small icebergs: drifting breakwaters in the Southern Ocean. *Ocean Modell* 1:2–7. <https://doi.org/10.1016/j.ocemod.2011.03.004>
- Ardhuin F, Roland A, Dumas F, Bennis A, Sentchev A, Forget P, Wolf J, Girard F, Osuna P, Benoit M (2012) Numerical wave modeling in conditions with strong currents: dissipation, refraction, and relative wind. *J Phys Oceanogr* 42:2101–2120. <https://doi.org/10.1175/JPO-D-11-0220.1>
- Ardhuin F, Gille ST, Menemenlis D, Rocha CB, Rasche N, Chapron B, Gula J, Molemaker J (2017) Small-scale open ocean currents have large effects on wind wave heights. *J Geophys Res*. <https://doi.org/10.1002/2016JC012413>
- Babanin AV, Hwung H, Shugan I, Roland A, der Westhuysen AV, Chawla A, Gautier C (2011) Nonlinear waves on collinear currents with horizontal velocity gradient. In: Proceedings of the 12th international workshop on wave hindcasting and forecasting and 3rd coastal hazards symposium, Big Island, Hawaii
- Benetazzo A, Carniel S, Sclavo M, Bergamasco A (2013) Wave–current interaction: effect on the wave field in a semi-enclosed basin. *Ocean Model* 70:152–165. <https://doi.org/10.1016/j.ocemod.2012.12.009>
- Bidlot JR, Abdalla S, Janssen P (2005) A revised formulation for ocean wave dissipation in cy25r1. Tech. Rep. 276, Research Dept. Tech. Rep. Memo. r60.9/JB/0516 ECMWF, Reading, United Kingdom
- Bolaños R, Brown JM, Souza AJ (2014) Wave–current interactions in a tide dominated estuary. *Cont Shelf Res* 87:109–123. <https://doi.org/10.1016/j.csr.2014.05.009>
- Bretherton FP, Garret CJR (1969) Wavetrains in inhomogeneous moving media. *Philos Trans R Soc Lond A* 302:529–554. <https://doi.org/10.1098/rspa.1968.0034>
- Caires S, Sterl A (2003) Validation of ocean wind and wave data using triple collocation. *J Geophys Res* 108(C3):3098. <https://doi.org/10.1029/2002JC001491>
- Chawla A, Kirby JT (2002) Monochromatic and random wave breaking at blocking points. *J Geophys Res* 107(C7). <https://doi.org/10.1029/2001JC001042>
- Chawla A, Spindler D, Tolman H (2012) Validation of a thirty year wave hindcast using the climate forecast system reanalysis winds. *Ocean Modelling* <https://doi.org/10.1016/j.ocemod.2012.07.005>, <http://linkinghub.elsevier.com/retrieve/pii/S1463500312001047> <http://www.sciencedirect.com/science/article/S1463500312001047>
- Chawla A, Spindler DM, Tolman HL (2013) Validation of a thirty year wave hindcast using the climate forecast system

- reanalysis winds. *Ocean Model* 70:189–206. <https://doi.org/10.1016/j.ocemod.2012.07.005>
- Cotton PD, Carter DJT (1994) Cross calibration of TOPEX, ERS-1, and GEOSAT wave heights. *J Geophys Res* 99:25,025–25,033. <https://doi.org/10.1029/94JC02131>
- Drennan WM, Shay LK (2006) On the variability of the fluxes of momentum and sensible heat. *Boundary Layer Meteorol* 119:81–107. <https://doi.org/10.1007/s10546-005-9010-z>
- Durrant TH, Greenslade DJM, Simmonds I (2009) Validation of Jason-1 and Envisat remotely sensed wave heights. *J Atmos Oceanic Technol* 26:123–134. <https://doi.org/10.1175/2008JTECH0598.1>
- Durrant TH, Greenslade DJM, Simmonds I (2013) The effect of statistical wind corrections on global wave forecasts. *Ocean Model* 70:116–131. <https://doi.org/10.1016/j.ocemod.2012.10.006>
- Durrant T, Greenslade D, Hemar M, Trenham C (2014) A global hindcast focussed on the Central and South Pacific. CAWCR Technical Report No. 070. ISSN: 1835-9884, ISBN: 9781486303175. http://www.cawcr.gov.au/technical-reports/CTR_070.pdf
- Hasselmann S, Allender KHJ, Barnett T (1985) Computation and parameterizations of the nonlinear energy transfer in a gravity-wave spectrum. part ii: parameterizations of the nonlinear energy transfer for application in wave models. *J Phys Oceanogr* 15:1378–1391. [https://doi.org/10.1175/1520-0485\(1985\)015<1378:CAPOTN>2.0.CO;2](https://doi.org/10.1175/1520-0485(1985)015<1378:CAPOTN>2.0.CO;2)
- Haus BK (2007) Surface current effects on the fetch-limited growth of wave energy. *J Geophys Res* 112(C03003). <https://doi.org/10.1029/2006JC003924>
- Hersbach H, Bidlot J (2008) The relevance of ocean surface current in the ECMWF analysis and forecast system. In: ECMWF Workshop on Ocean-atmosphere interactions, Camp Springs, MD, pp. 61–73. <http://www.ecmwf.int/sites/default/files/elibrary/2009/9866-elevance-ocean-surface-current-ecmwf-analysis-and-forecast-system.pdf>
- Janssen PAEM (1991) Quasi-linear theory of wind wave generation applied to wave forecasting. *J Phys Oceanogr* 21:1631–1642. [https://doi.org/10.1175/1520-0485\(1991\)021<1631:QLTOWW>2.0.CO;2](https://doi.org/10.1175/1520-0485(1991)021<1631:QLTOWW>2.0.CO;2)
- Kenyon KE (1971) Wave refraction in ocean currents. *Deep-Sea Res* 18:1023–1034. [https://doi.org/10.1016/0011-7471\(71\)90006-4](https://doi.org/10.1016/0011-7471(71)90006-4)
- Komen GJ, Hasselmann S, Hasselmann K (1984) On the existence of a fully developed wind–sea spectrum. *J Phys Oceanogr* 14:1271–1285. [https://doi.org/10.1175/1520-0485\(1984\)014<1271:OTEOAF](https://doi.org/10.1175/1520-0485(1984)014<1271:OTEOAF)
- Kudryavtsev VN, Grodsky SA, Dulov VA, Bol'shakov AN (1995) Observation of wind waves in the Gulf Stream frontal zone. *J Geophys Res* 100(C10). <https://doi.org/10.1029/95JC00425>
- Longuet-Higgins MS, Stewart RW (1961) The changes in amplitude of short gravity waves on steady non-uniform currents. *J Fluid Mech* 10(04):529–549
- Mathiesen M (1987) Wave refraction by a current whirl. *J Geophys Res* 92:3905–3912. <https://doi.org/10.1029/JC092iC04p03905>
- Meyers G (2008) The Australian integrated marine observing system. *J Atmos Oceanic Technol* 3:80–81. <https://doi.org/10.1175/JTECH-D-10-05033>
- Peregrine DH (1976) Interaction of water waves and currents. *Adv Appl Mech* 16:9–117
- Queffelec P, Croizé-Phillon D (2014) Global altimeter SWH data set, Version 11, Tech. Rep., IFREMER, France. ftp://ftp.ifremer.fr/ifremer/cersat/products/swath/altimeters/waves/documentation/altimeter_wave_merge_11.pdf
- Rapizo H, Babanin A, Gramstad O, Ghantous M (2014) Wave refraction on Southern Ocean eddies. In: Proceedings of the 19th Australasian Fluid Mechanics Conference, Melbourne, p 4p. <http://people.eng.unimelb.edu.au/imarusic/proceedings/19/18.pdf>
- Rapizo H, Babanin AV, Schulz E, Hemer M, Durrant TH (2015) Observation of waves from a moored buoy in the Southern Ocean. *Ocean Dynam* 65:1275–1288. <https://doi.org/10.1007/s10236-015-0873-3>
- Rapizo H, Waseda T, Babanin AV, Toffoli A (2016) Laboratory experiments on the effects of a variable current field on the spectral geometry of water waves. *J Phys Oceanogr* 46:2695–2717. <https://doi.org/10.1175/JPO-D-16-0011.1>
- Rapizo H, Babanin AV, Provis D, Rogers WE (2017) Current-induced dissipation in spectral wave models. *J Geophys Res* 122:2205–2225. <https://doi.org/10.1002/2016JC012367>
- Raschle N, Ardhuin F (2013) A global wave parameter database for geophysical applications. Part 2: model validation with improved source term parameterization. *Ocean Modell* 70:174–188. <https://doi.org/10.1016/j.ocemod.2012.12.001>, <http://linkinghub.elsevier.com/retrieve/pii/S1463500312001709>
- Ris RC, Holthuijsen LH (1996) Spectral modelling of current wave-blocking. In: Proceedings of the 25th International Conference on Coastal Engineering, Orlando, pp 1247–1254
- Saha S et al (2010) The NCEP climate forecast system reanalysis. *Bull Amer Meteor Soc* 91:1015–1057. <https://doi.org/10.1175/2010BAMS3001.1>
- Schulz E, Josey SA, Vereen R (2012) First air-sea flux mooring measurements in the southern ocean. *Geophys Res Lett* 39:8. <https://doi.org/10.1029/2012GL052290>
- Stopa JE, Cheung KF (2014) Intercomparison of wind and wave data from the ECMWF reanalysis interim and the NCEP climate forecast system reanalysis. *Ocean Model* 75:65–83. <https://doi.org/10.1016/j.ocemod.2013.12.006>
- Stopa JE, Ardhuin F, Babanin AV, Zieger S (2016) Comparison and validation of physical wave parameterizations in spectral wave models. *Ocean Model* 103:2–17. <https://doi.org/10.1016/j.ocemod.2015.09.003>
- Tolman HL (1990) The influence of unsteady depths and currents of dikes on wind-wave propagation in shelf seas. *J Phys Oceanogr* 20:1166–1174
- Tolman HL (1991) A Third-Generation model for wind waves on slowly varying, unsteady, and inhomogeneous depths and currents. *J Phys Oceanogr* 21(6):782–797. [https://doi.org/10.1175/1520-0485\(1991\)021<0782:ATGMFW>2.0.CO;2](https://doi.org/10.1175/1520-0485(1991)021<0782:ATGMFW>2.0.CO;2)
- Tolman HL (2002) Validation of WAVEWATCH III version 1.15 for a global domain. Tech Note 213, NOAA/NWS/NCEP/MMAB
- Van der Westhuysen AJ (2012) Spectral modeling of wave dissipation on negative current gradients. *Coast Eng* 68:17–30
- Waseda T, Kinoshita T, Cavaleri L, Toffoli A (2015) Third-order resonant wave interactions under the influence of background current fields. *J Fluid Mech* 784:51–73. <https://doi.org/10.1017/jfm.2015.578>
- White B, Fornberg B (1998) On the chance of freak waves at sea. *J Fluid Mech* 355:113–138
- Zieger S, Babanin AV, Rogers WE, Young IR (2015) Observation-based source terms in the third-generation wave model WAVEWATCH. *Ocean Model* 96:2–25. <https://doi.org/10.1016/j.ocemod.2015.07.014>